Chaos, Solitons and Fractals 130 (2020) 109465

Contents lists available at ScienceDirect

Chaos, Solitons and Fractals

Nonlinear Science, and Nonequilibrium and Complex Phenomena

journal homepage: www.elsevier.com/locate/chaos

Frontiers

Anisotropy of acoustic emission in coal under the uniaxial loading condition

Honghua Song[a,d,*], Yixin Zhao[a,c,d,*], Derek Elsworth[d], Yaodong Jiang[b,c], Jiehao Wang[d]

[a] College of Resources and Safety Engineering, China University of Mining and Technology, Beijing, China
[b] School of Mechanics and Civil Engineering, China University of Mining and Technology, Beijing, 100083, China
[c] State Key Laboratory of Coal Resources and Safe Mining, China University of Mining and Technology, Beijing, 100083, China
[d] Energy and Mineral Engineering, G3 Center and EMS Energy Institute, Pennsylvania State University, University Park, PA, USA

ARTICLE INFO

Article history:
Received 14 November 2018
Revised 14 July 2019
Accepted 26 September 2019
Available online 9 October 2019

Keywords:
Coal
Acoustic emission
Anisotropy
Computed tomography
Uniaxial compressive loading

ABSTRACT

We explore microstructure-related anisotropy of acoustic emission (AE) in coal and investigate connections to time-sequence-related fractal dimension (TRFD) and AE parameters of counts and cumulative energy. We characterize microstructure and anisotropy by imaging via X-ray CT. The anisotropic features of AE in coal are measured during uniaxial compression on a series of coal samples with varying inclinations of the anisotropy (bedding plane) relative to the loading direction (0°, 15°, 30°, 45°, 60°, and 90°). The form of the cumulative absolute AE energy released during loading is U-shaped with respect to increasing anisotropic angle. The maximum cumulative absolute AE energy occurs at an anisotropic angle of 90° (perpendicular to loading) and the minimum magnitude is when loading is at 45°. Cumulative AE counts have a complex structure with bedding plane inclination, decreasing to a minimum at an anisotropic angle of 30°, and peaking at 45° with terminal AE counts at 0° and 90° intermediate between these. The TRFD correlates positively with the cumulative AE counts with a trough at 15° and peak at 45°. The greater value of the TRFD in coal indicates a more uniform distribution of the AE count in time sequence, a smaller difference in the number of AE count between each time interval and less AE energy dissipated during the loading process. A theoretical basis for the observed negative exponential correlation between TRFD and AE energy dissipation during the loading process is developed. In samples with different anisotropic angles, this correlation conforms to the empirical relations that developed based on the space-related fractal dimension (SRFD) and AE energy dissipated by micro-seismic events recorded in situ.

1. Introduction

Acoustic emission (AE) is generated by the rapid growth and interaction of micro-cracks [1,2] and as a ubiquitous phenomenon associated with the brittle fracture [3,4]. AE provides a wealth of information regarding the failure process in coal and rock [5]. Investigating the features of the AE distribution in space and time yields important constraint on failure process in coal and rock. This provides constraint on the nucleation and propagation of micro-cracks [6], characteristics of crack growth [7], evaluation of damage [8–10], information on energy dissipation and the seismic features of micro-earthquakes [11,12], and the monitoring and forecasting of dynamic failure in coal mines [13].

In rock mechanics, the AE experiment was initiated as part of a study on problems associated with mine design and alleviation of rock bursts or coal bump, since the late 1930s [14]. More recently the AE technique had been increasingly employed to the laboratory study of basic deformation and failure mechanisms in geologic materials and the field usage with the consideration of the micro seismic activities. In general, AE in coal and rock is affected by the grain size [15], and the presence of pores [16], bedding planes [17], and pre-existing discontinuities [18]. The anisotropic features of microstructures may exert a significant influence on the AE forms in coal when loaded in different directions [19], understanding the anisotropic AE features in coal is beneficial for the micro seismic signal analysis, the coal bump forecasting, and the coal failure-related activities during the mining processes. However, this aspect of response has not been extensively investigated, and correspondingly is not well characterized.

X-ray computed tomography (X-CT) is a nondestructive imaging technique [20,21] that may be applied to define structure and

* Corresponding authors.
E-mail addresses: honghuasong8@hotmail.com (H. Song), zhaoyx@cumtb.edu.cn (Y. Zhao).

https://doi.org/10.1016/j.chaos.2019.109465
0960-0779/

illuminate failure processes [22,23]. The combination of X-CT and advanced data reduction models enables nondestructive characterization of structure [24].

Acoustic emission has fractal features in space, time and magnitude distribution [1,25]. This provides an approach to quantitatively distinguish the AE features generated during deformation and failure of coal and to develop correlations in response that are applicable to different loading conditions. The temporal sequence and spatial distribution of the AE are two series of data that may be used to define fractal dimensions of the AE cloud [26,27]. The space distribution related fractal dimension (SRFD) is broadly used in both laboratory and field measurements and its application in the failure of coal has been widely investigated in developing connections between SRFD and AE dissipation [10,27]. However, due to the complexity in both measuring and locating AE events, for the calculation of SRFD, the usage of the time sequence related fractal dimension (TRFD) is becoming popular.

Thus, to reveal the microstructure-related anisotropy of AE in coal, microstructures in coal are first characterized by X-ray CT, and then subject to destructive uniaxial compression tests with concurrent AE measurement. This is completed on a series of coal specimens with bedding anisotropic angles of 0°, 15°, 30°, 45°, 60°, and 90° (relative to the loading direction) with the TRFD for each angle of anisotropy calculated and used to correlate with other observed AE parameters. These observations are used to build mechanistically-driven correlations in response.

2. Methodology

A series of coal samples with different inclinations of anisotropy are prepared. Interior structure is obtained via X-ray CT with the features of the AE response measured under uniaxial deformation, through failure.

2.1. Properties of coal

The block coal samples used in this research are from the No. 45 coal seam of the Wudong Mine, Xinjiang Province, China. The samples are wrapped at the working face in water-polycrylic resin to prevent oxidation and drying during transportation. The density of the coal is 1.46 g/cm^3, and the moisture content is 1.8%. Mineral matter is present in minor proportions (8.2%), comprising kaolinite (62.0%), nacrite (26.5%), lizardite (10.8%), and Pentahydroborite (0.4%), as defined by X-ray diffraction. The block coal used in this research has a low metamorphism degree and belongs to long flame coal, with vitrinite reflectance of 0.5–0.64%, ash (11.97–24.56%), volatile matter (39.48–47.12%), and floating coal volatiles (38.40–42.77%) as determined by the proximate analysis.

2.2. Specimen process

Standard cylindrical specimens are prepared with length to diameter ratio of two [28] and diameters of 25 mm. A total of twenty specimens are prepared with orientations of the bedding planes inclined with angles of 0°, 15°, 30°, 45°, 60°, and 90° with respect to the loading direction. To ensure the accuracy of the anisotropic angles and improve the success rate during the specimen drilling process, coal blocks were firstly trimmed to make the inclination of bedding plane relative to the vertical direction equal to corresponding anisotropic angles, and then fixing the coal block and drilling vertically. Coal samples and a schematic diagram of the anisotropic angle are shown in Fig. 1.

2.3. X-ray CT scanning

Due to the sedimentary process and the geological movement during the coal formation, mineral inclusions and cleats are randomly existed in coal, while the orientation of them in coal blocks are certain in an area and can be reasonably revealed by the X-ray CT scanning result of a specimen [29,30]. Thus, a specimen with an anisotropic angle of 0° is scanned in this experiment to obtain the orientation anisotropy of microstructures in these specimens. The micro X-ray CT scanner used in this experiment is NanoVoxel 4000 (Sanying, China). It is a high power micro-CT system using a high voltage X-ray source (225 kV, 240 kV and 300 kV are optional) with sub-micron spatial resolution (≤0.5 μm). The voltage used here is 225 kV, and the spatial resolution is 0.5 μm.

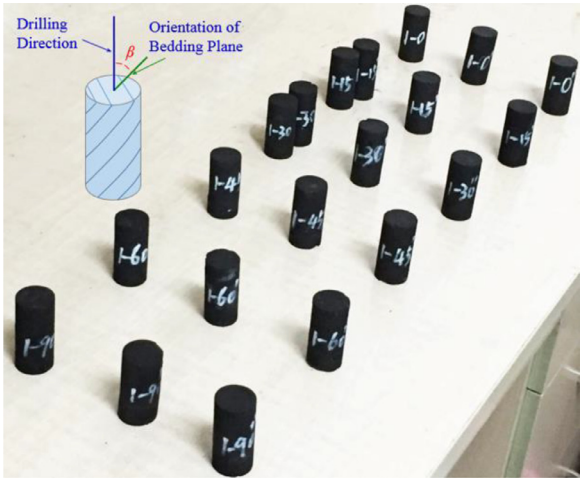

Fig. 1. Coal samples and the anisotropic angle (β): (a) the anisotropic angle used in this article; (b) coal specimens with different anisotropic angles.

2.4. Uniaxial compression test and AE measurement

After CT scanning, uniaxial compression tests are conducted on a double controlled electronic universal testing machine, WDW-100E, with a capacity of 100 kN and a displacement precision of ±0.5%. The tests are at room temperature and under displacement-control at 1 mm/min.

The AE signal is recorded by a PCI-2 device (Physical Acoustic Corporation-PAC) in waveform streaming mode. The AE testing set-up consists of 4 Micro 30S sensors (10 mm in diameter) and a 6-type preamplifier. The bandwidth frequency is 1 kHz∼3 MHz with a maximum signal amplitude of 100 dB with a dynamic range greater than 85 dB.

3. Results and discussion

We characterize the distribution of microstructures in coal and define the anisotropic features of the AE response (space, time and frequency-magnitude) and relate this to the uniaxial compressive strength (UCS).

3.1. Microstructural characterization of coal

A series of CT images obtained from X-ray CT scanning are used to define and reconstruct the interior structure of the coal as shown in Fig. 2. Mineral inclusions, pre-existing discontinuities (cleats and cracks) are the two main microstructures present in coal, as that exists in other coal [31,32], as shown in Fig. 2. The orientation of mineral inclusions and bedding plane cracks are parallel to the bedding plane with cleats near perpendicular to the bedding plane.

Since the anisotropic angle is defined as the angle of drilling direction relative to the orientation of the bedding plane, as shown in Fig. 1, thus, the orientation of bedding plane cracks and the

Fig. 2. Distribution of mineral inclusions and initial cracks within a coal sample.

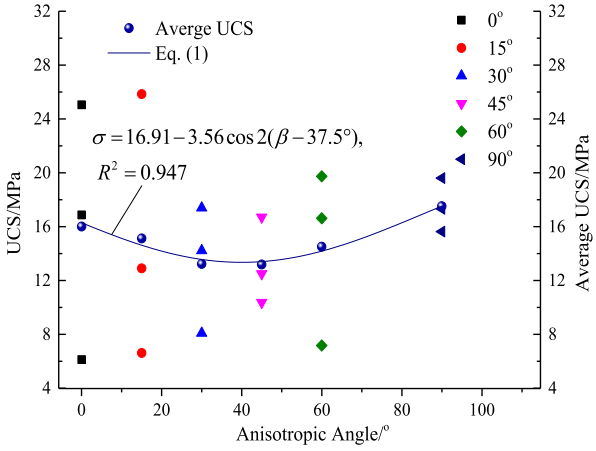

Fig. 3. The UCS of coal specimens with different anisotropic angles and the UCS-Anisotropic angle curve.

bedding plane share the same anisotropic angle (β) relative to the loading direction, while the cleats have an angle close to ($90°-\beta$) with the loading direction since it near perpendicular to the bedding plane. Meanwhile, due to the orientation of bedding plane, mineral inclusions, pre-existing discontinuities (cleats and bedding plane cracks), and the angles among them in coal blocks used in this experiment have consistency, the inclination of loading direction with respect to the orientation of these microstructures (bedding plane, mineral inclusions, and pre-existing discontinuities) in coal are regularly changes with the anisotropic angles.

3.2. Uniaxial compressive strength

Uniaxial compressive strength (UCS) is a fundamental mechanical parameter of coal. Based on the foregoing classification on UCS-Anisotropic angle curves, the average UCS in this experiment is a U-shaped curve relative to the anisotropic angle, as shown in Fig. 3. It reaches the maximum value (17.52 MPa) at an anisotropic angle of 90° with a minimum value (13.19 MPa) returned at an anisotropic angle of 45°. This is consistent with the strength anisotropy of other coals obtained by Pomeroy et al. [33] and some stratified rocks [34]. Eq. (1) is used for the U-shaped curve verification, since it describes the variation of the UCS with anisotropic angles with U-shaped feature [29].

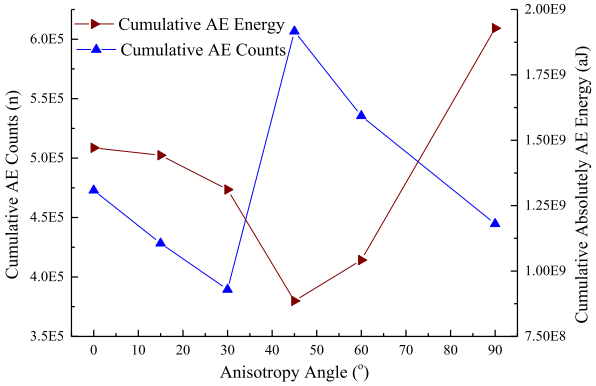

Fig. 4. Comparison of average cumulative acoustic emission (AE) counts and absolutely energy in coal samples with different angles of anisotropy.

$$\sigma = E - F\cos 2(\beta - \beta_{\min}) \quad (1)$$

where σ is the average UCS at the anisotropic angle of β; β_{min} is the anisotropic angle where the UCS is minimum; E and F are constants relating to the friction angle of coal. The fitting curve in Fig. 3 shows a good correlation with the experimental data and the regression coefficient is 0.947, which indicates the UCS-Anisotropic curve in this experiment is U-shaped. However, the U-shape type of the curve in Fig. 3 is less obvious, this mainly caused by the greater ordinate value range chosen in Fig. 3 to guarantee all the UCS point are exhibited.

The form of the strength anisotropy in coal demonstrates that the weakness plane, comprising bedding plane cracks, mineral inclusions, and fining cycles, dominates the strength of coal [33,35], as shown in Fig. 2. This is attributed to the periodical variation of the fracture toughness and shear strength across the weakness plane [36]. Since the distribution of mineral inclusions and the orientation of bedding plane cracks are parallel to that of bedding plane, the orientation of bedding plane can be considered as the dominant factor controlling the strength anisotropy of coal.

3.3. Anisotropy of AE in coal

The AE count, AE energy, and fractal dimension are three fundamental parameters that describing the AE features of coal and rock [37,38]. In general, the cumulative AE counts and absolute AE energy reveal the overall difference in AE response when loaded at different angles, while the fractal dimension indirectly reflects the AE characteristics in time and space during the loading process [39].

We use the average cumulative AE counts and absolute AE energy to illustrate the specific anisotropic features of AE in coal, here the absolute AE energy is calculated based on the duration, the sampling voltage of the analog-to-digital converter (ADC), and the impedance, namely, absolute AE energy = sum (ADC sample voltage)^2 / impedance. The cumulative absolute AE energy is positively correlated with the UCS, as shown in Figs. 3 and 4. The average cumulative absolute AE energy released during the entire loading process is U-shaped relative to the increasing anisotropic angle, although it approximately remains constant as the anisotropic angle increases from 0° to 30°. The average cumulative absolute AE energy is maximum when the anisotropic angle is 90° (1.93×10^9 aJ) and is minimum at the anisotropic angle of 45° (8.85×10^8 aJ).

AE counts reduce with an increase of anisotropic angle within the range 0°–30° and reach a minimum at 30° (3.89×10^5). Beyond

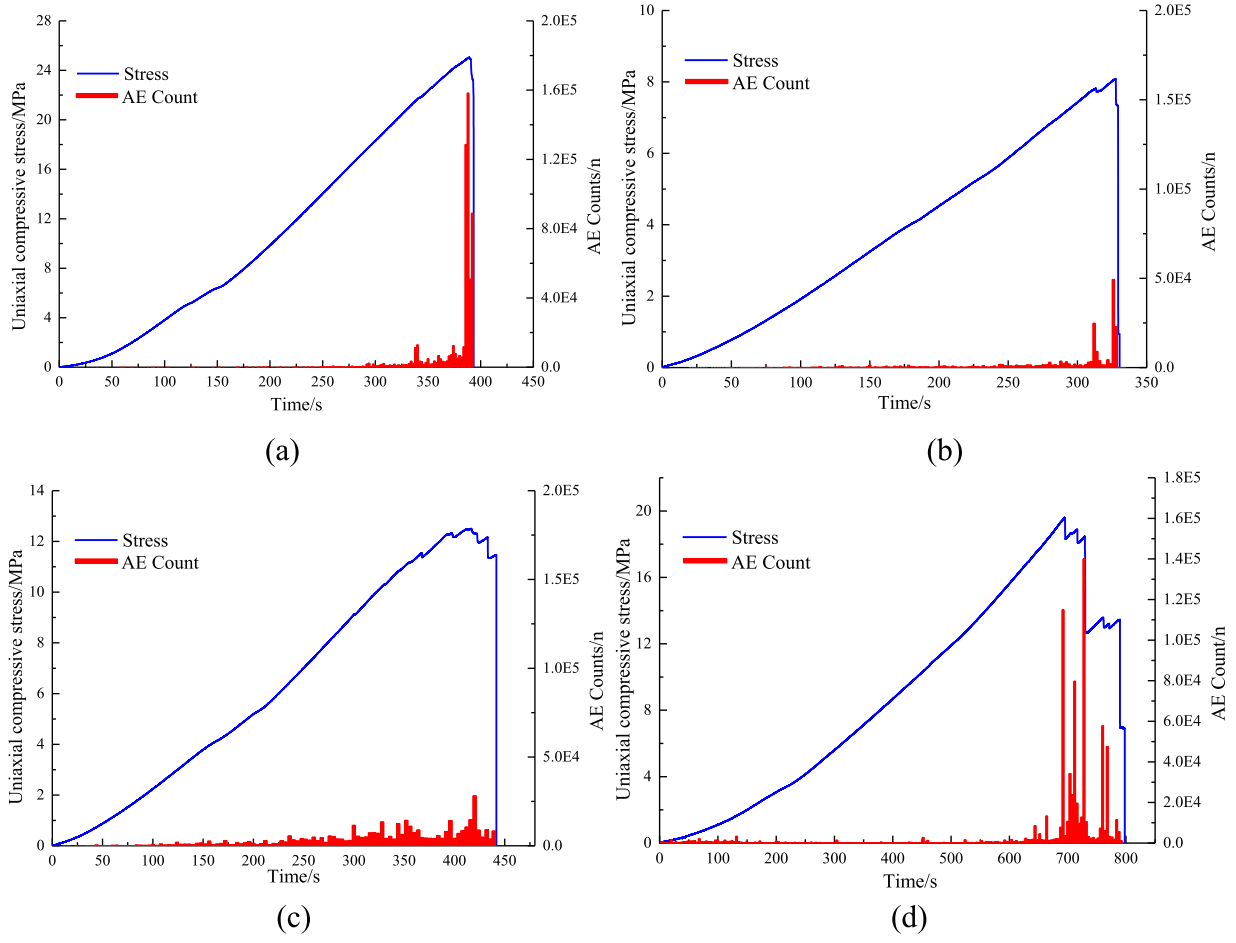

Fig. 5. AE counts during the entire loading process when loading samples with different angles of anisotropy: (a) 0°; (b) 30°; (c) 45°; (d) 90°.

that, the counts increase sharply to a maximum at an anisotropic angle of 45° (6.06×10^8), before then decreasing as the anisotropic angle further increases, as shown in Fig. 4.

The cumulative absolute AE energy response in coal is related to the orientation of weakness plane. Based on the positive correlation of the UCS and stress needed for crack initiation [40], the analogous anisotropic feature of fracture toughness and UCS [41], and the variation of bulk friction with bedding plane orientation [42], the stress required for crack initiation along the weakness plane should have a U-shaped form. In other words, the curve should decrease to a minimum at an anisotropic angle of 0° to (45°−φ/2), where φ is the friction angle [29], and then increase to a maximum at 90°. Thus, the energy accumulated around cracks before crack initiation should be a similar U-shape pattern relative to the anisotropic angle. This contributes to the U-shaped curve of the average cumulative absolute AE energy against the angle of anisotropy, since the AE energy dissipated during the failure process is positively correlated with the fracture energy released due to the crack initiation [25,43,44].

The anisotropy of the cumulative AE counts is dominated by the influence of the bedding plane due to the decrease of the stress threshold for crack initiation as the anisotropic angle increases from 0° to 30°. This results in an increase in AE counts generated before this progressive failure, fewer AE counts produced during progressive failure, and a shorter time needed for the entire failure of the specimen [17,45], as shown in Figs. 5(a) and (b). Thus, less cumulative AE counts are detected when the anisotropic angle increases from 0° to 30°, since last two factors exert more impact on the number of AE counts generated during the loading process.

The dramatic increase in the cumulative AE counts when the anisotropic angle is in the range 30°–45° is affected by both bedding plane and cleats. Since the weakness plane is parallel to the bedding plane and cleats are perpendicular, angles between the orientation of cleats and weakness plane and the loading direction are closer to the critical (45°−φ/2) than the other angle of anisotropy, as shown in Fig. 2. Thus, higher AE counts are measured before progressive failure, and greater cumulative AE counts are obtained within this range of the anisotropic angle.

The reduction of cumulative AE counts, as the anisotropic angle increases from 45° to 90°, is attributed to the increasing inclination of weakness plane. The initiation stress threshold for cracks that parallel the bedding plane increases with the anisotropic angle within this range of anisotropic angles. This contributes to less AE counts produced before progressive failure, with more energy accumulated around cracks, and greater AE counts measured at the rapid failure process, as shown in Fig. 5(d). Thus, the cumulative AE counts in specimens show a reduction with an increase in the anisotropic angle under the mutual influence of these two factors.

4. Fractal features of AE in time sequences

Fractal dimensions of AE in coal samples with different inclinations of bedding planes are calculated, based on the time sequence related AE count. The anisotropy of the fractal dimension of AE is summarized and correlations between TRFD and other AE parameters are explored.

4.1. Theoretical development

The correlation dimension was initially developed by Grassberger and Procaccia (G–P) [26,27], based on embedding and phase space reconstruction theory. The correlation dimension (D) describes the dispersion degree of fractal objects [46], as cracks, AE events, and micro seismicity. Since its development, the correlation dimension has been broadly used to describe the fractal features of AE in brittle materials. The construction of the dimension space is the most important part for the calculation of the correlation dimension.

In this work, the phase space is reconstructed on the basis of an experimentally acquired time sequence of AE counts with fractal dimension evaluated via the G-P algorithm. For a certain time sequence of AE counts $X_n = \{x_1, x_2, ..., x_n\}$, where n is the number of points in the time sequence X_n. If an appropriate embedding dimension m ($m < n$) and the time hysteresis parameter t are selected, the reconfigurable phase space can be expressed by a series of vectors that are sequentially taken from X_n with a length of m [17,26], namely

$$Y_i = \left\{x_i, x_{(i+t)}, \ldots, x_{(i+(m-1)t}\right\} \quad (i = 1, 2, 3, \ldots, (n-m+1)) \quad (2)$$

where Y_i is any vector in the phase space.

The correlation integral is the probability that distances between any two vectors in the m-dimension phase space is less than r, after the construction of the phase dimension, and can be calculated by

$$C(r) = \frac{1}{N(N-1)} \times \{\text{No. of pairs } (Y_i - Y_j) \text{ with } \left|Y_i - Y_j\right| < r\}, (i \neq j). \quad (3)$$

In general, the standard correlation function is expressed as

$$C(r) = \frac{1}{N(N-1)} \sum_{i=1}^{N} \sum_{j=1}^{N} H(r(k) - \left|Y_i - Y_j\right|), (i \neq j) \quad (4)$$

where $C(r)$ is the correlation integral, N are the number of vectors in the m-dimension phase space, $r(k)$ is the given scale function that can be obtained as

$$r(k) = kr, r = \frac{1}{n(n-1)} \sum_{i=1}^{n} \sum_{j=1}^{n} \left|Y_i - Y_j\right|, (i \neq j) \quad (5)$$

where r is the average distance of two arbitrary vectors in the m-dimension phase space, where each $r(k)$ has a $C(r)$ corresponding to it, k is the scaling factor and H is the Heaviside function, of the form,

$$H(x) = \begin{cases} 1, & x \geq 0 \\ 0, & x < 0 \end{cases}. \quad (6)$$

If the acoustic emission has a fractal structure, the relation between $C(r)$ and r can be described as,

$$C(r) \propto r^D. \quad (7)$$

If the value of r is within a reasonable range, the relation between $C(r)$ and r can also be transformed as

$$\ln C(r) = C + D \ln r \quad (8)$$

where D is the correlation dimension, namely the slope of the function ln C(r)-ln$r$ curve where C is a constant.

Parameters m and k are significant in the correlation dimension calculated by the G-P algorithm. In general, the correlation dimension D increases with m, and asymptotes to a constant when m is greater than a critical value [17]. Meanwhile, k determines the number of vector pairs whose separation distance is greater than $r(k)$, and it thereby affects the variation of $C(r)$ and the value of D. Since the correlation dimension D is obtained by the regression analysis, based on a series of r and corresponding $C(r)$, as indicated by Eq. (8), thus, a series of k must be reasonably selected to make the correlation dimension distinctively reflects the fractal feature of each AE process in a series of experiments. In this work, the value of m is chosen as 4, and a series of k with values of 0.1, 0.2, ..., 1.2, twelve k in total (with a value interval of 0.1), are determined after multiple attempts.

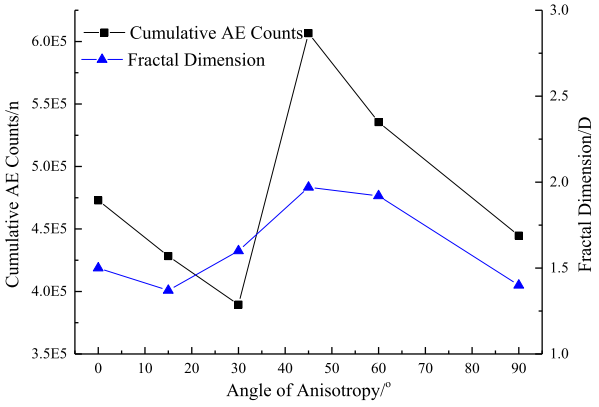

Fig. 6. Anisotropy of fractal dimension of coal samples loaded in various directions.

4.2. Fractal anisotropy of AE in coal

The value of time sequence related fractal dimensions (TRFD) of specimens with different anisotropic angles is positively correlated with the cumulative AE counts, as shown in Fig. 6. The average value of fractal dimension reduces from 1.50 to 1.37 as the anisotropic angle within 0°–15°, and then increases to a peak at an anisotropic angle of 45°, following which it decreases to 1.40 as the angle of anisotropy increases to 90°.

Based on the fractal theory developed in the previous section, the greater value of TRFD indicates a smaller scatter of the vector lengths in the m-dimensional phase space. This represents a more uniform distribution of the AE count in the time sequence and smaller differences of AE count in every time interval, as apparent in the anisotropy of the AE fractal dimension shown in Fig. 6 and the AE feature plotted in Fig. 5.

The smaller value of TRFD represents the greater concentration of the AE count during the progressive failure, as the stress-time and AE count-time curves show in Figs. 5(a) and (d). This also indicates that greater AE energy dissipates during the loading process (Fig. 4). Meanwhile, the reducing trend of TRFD in coal is consistent with the variation of b ($b = 2D$) in rocks and concretes as the AE energy dissipation gains [47,48]. This reveals the applicability of the TRFD in describing the time sequence related distribution and energy dissipation feature of AE counts during the loading process.

4.3. Relationship between cumulative AE energy and TRFD

The relation between fractal dimension and AE energy dissipated during the loading process is significant in the prevention of dynamic failures (rock bursts) in coal mines [10,27]. A theoretical correlation between TRFD and cumulative AE energy dissipation during the loading process is investigated in the following.

Based on the correlation dimension theory introduced in the previous section, the AE energy dissipated in any vector of the m-dimension phase space can be expressed as

$$E_i = \alpha_i ||Y_i|| \quad (9)$$

where $\|Y_i\|$ is the number of AE counts in the vector of Y_i, α_i is the average energy released in each AE count of Y_i, E_i is the cumulative

AE energy dissipated by a vector of the m-dimension phase space ($i=1, 2, \ldots,(n-m+1)$).

Since the time sequence related AE counts during the failure process has fractal features, based on the definition of fractal geometry [27,49], namely the power-law [49], the number of vectors with AE counts greater than that in Y_i should be

$$\phi(Y_i) \sim ||Y_i||^{-\frac{D}{2}} \tag{10}$$

where D is the fractal dimension. Thus, once a reasonable vector Y_i and corresponding α_i in the m-dimension space are chosen, the amount of energy E dissipated during the whole loading process can be approximately expressed as

$$E \sim \frac{1}{m}\phi(Y_i)E_i = \frac{1}{m}\phi(Y_i)\alpha_i||Y_i|| \tag{11}$$

Namely, the AE energy dissipation can be represented by the space dimension value m, the AE energy dissipation in a vector (E_i) and the amount of vector with AE counts greater than it ($\phi(Y_i)$). Replace the $\phi(Y_i)$ by Eq. (10), the Eq. (11) can be transferred as

$$E \sim \frac{1}{m}\alpha_i||Y_i||^{1-\frac{D}{2}} \tag{12}$$

where m is the dimension of phase space in the TRFD. Obviously, the TRFD exhibits a negative exponential correlation with the cumulative AE energy dissipated during the loading process. This is consistent with value of TRFD plotted in Fig. 6 and the cumulative absolute AE energy shown in Fig. 4.

Meanwhile, the correlation of TRFD and the cumulative AE energy revealed by Eq. (12) has a similarity with that of the SRFD and the energy dissipation of the microseismicity in coal mines [27]. It is also consistent with the energy–fractal dimension relations defined by the Gutenberg-Richter relation (also called the magnitude-frequency relation) of natural tectonic earthquakes, namely greater fractal dimension indicates smaller energy dissipation [50]. This manifests the TRFD is also capable in revealing the AE features of microseismic records and in understanding seismic precursors to collapse in coal mines.

However, since the variation of Y_i in Eq. (12) will differ as the coal specimen changes, a more general expression is needed to describe the correlation of TRFD and cumulative AE energy for coal samples exhibiting different anisotropic angles. In considering the similarity observed in the energy-fractal dimension feature of the TRFD and the SRFD in the microseismicity of coal mines, the relation of TRFD and cumulative AE energy for coal samples with different anisotropic angles may be analyzed based on the empirical equation summarized by Xie and Pariseau [27], namely,

$$D = C_1 \times \exp[-C_2 E] \tag{13}$$

where C_1 and C_2 are constants varying with the mechanical properties and anisotropic angles of coal specimen, the fractal dimension D ranges from 0.0 to 3.0, E is the average cumulative absolute AE energy, and D is the average fractal dimension in each loading direction.

The regression results shown in Fig. 7 indicate the applicability of Eq. (13) in revealing the relationship between the TRFD and cumulative absolute AE energy dissipated during the loading process in coal samples with different anisotropic angles - since the curve fits well with the experimental data with a correlation coefficient (R^2) is 0.78.

In addition, Eq. (13) also provides a potential approach for investigating the relation between TRFD and AE energy dissipated by microseismicity during the coal mining process, based on a series of laboratory uniaxial compressive experiments and the consideration of scale effect.

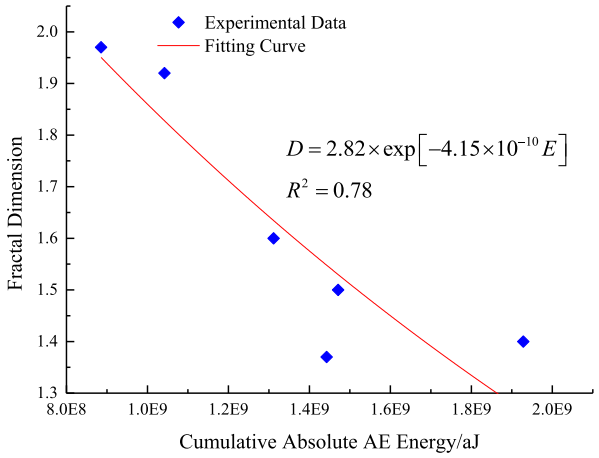

Fig. 7. Fitting result of fractal dimension and cumulative absolute energy based on Eq. (13).

5. Conclusion

We characterize the microstructure related anisotropy of AE in coal, based on the measurement of AE response on a series of coal samples with anisotropic angles of 0°, 15°, 30°, 45°, 60°, and 90°. This is measured under uniaxial compression together with X-ray CT imaging. These data are used to evaluate the time sequence related fractal dimension of the AE signals using the G–P algorithm. We use this to explore the fractal anisotropy of AE and the connection between TRFD and other parameters on acoustic emission during the loading process. The conclusions are summarized as below:

a. The cumulative absolute energy has a U-shape form with increasing anisotropic angle. The maximum value is observed at an anisotropic angle of 90° with a minimum value at an anisotropic angle of 45°. Unlike this distribution, the cumulative acoustic counts exhibit a trough at an anisotropic angle of 30° and peaks at an anisotropic angle of 45°. The orientation of the bedding planes dominate the anisotropy of average cumulative absolute energy, while the variation of average cumulative AE counts is affected by both bedding plane and cleats.
b. The TRFD is positively correlated with the cumulative AE counts. It also has a peak and trough with maximum at 45° and a minimum at 15°. The greater value of TRFD indicates a more uniform distribution of AE counts in the time sequence, a smaller difference in the number of AE counts during each time interval and less AE energy dissipated during the loading process.
c. The TRFD has a negative exponential correlation with the cumulative AE energy dissipation. Furthermore, this correlation in different specimens with different angles of anisotropy is similar to the empirical equation summarized by former researchers on the basis of the SRFD and AE energy dissipated by micro seismicity in the coal mining process.

Declaration of Competing Interest

The authors declare that they have no known competing financial interests or personal relationships that could have appeared to influence the work reported in this paper.

Acknowledgments

This research is supported by the National Key R&D Program of China (2016YFC0801401 and 2016YFC0600708), Yue Qi Distin-

guished Scholar Project of China University of Mining & Technology(Beijing) and Fundamental Research Funds for the Central Universities.

References

[1] Lockner D. The role of acoustic emission in the study of rock fracture. Int J Rock Mech Min Sci Geomech Abstr 1993;30:883–99. https://doi.org/10.1016/0148-9062(93)90041-B.

[2] He MC, Miao JL, Feng JL. Rock burst process of limestone and its acoustic emission characteristics under true-triaxial unloading conditions. Int J Rock Mech Min Sci 2010;47:286–98. doi:10.1016/j.ijrmms.2009.09.003.

[3] Kietov V, Henschel S, Krüger L. Study of dynamic crack formation in nodular cast iron using the acoustic emission technique. Eng Fract Mech 2018;188:58–69. doi:10.1016/j.engfracmech.2017.07.009.

[4] Codeglia D, Dixon N, Fowmes GJ, Marcato G. Analysis of acoustic emission patterns for monitoring of rock slope deformation mechanisms. Eng Geol 2017;219:21–31. https://doi.org/10.1016/j.enggeo.2016.11.021.

[5] Nasseri MHB, Goodfellow SD, Lombos L, Young RP. 3-D transport and acoustic properties of Fontainebleau sandstone during true-triaxial deformation experiments. Int J Rock Mech Min Sci 2014;69:1–18. doi:10.1016/j.ijrmms.2014.02.014.

[6] Yuan R fu, hui Li Y. Fractal analysis on the spatial distribution of acoustic emission in the failure process of rock specimens. Int J Miner Metall Mater 2009;16:19–24. doi:10.1016/S1674-4799(09)60004-2.

[7] Filipussi D, Piotrkowski R, Ruzzante J. Characterization of a crack by the acoustic emission signal generated during propagation. Procedia Mater Sci 2012;1:266–72. https://doi.org/10.1016/j.mspro.2012.06.036.

[8] Carpinteri A, Lacidogna G, Pugno N. Structural damage diagnosis and life-time assessment by acoustic emission monitoring. Eng Fract Mech 2007;74:273–89. https://doi.org/10.1016/j.engfracmech.2006.01.036.

[9] Su G, Shi Y, Feng X, Jiang J, Zhang J, Jiang Q. True-Triaxial experimental study of the evolutionary features of the acoustic emissions and sounds of Rockburst processes. Rock Mech Rock Eng 2018;51:375–89. doi:10.1007/s00603-017-1344-6.

[10] Xie HP, Liu JF, Ju Y, Li J, Xie LZ. Fractal property of spatial distribution of acoustic emissions during the failure process of bedded rock salt. Int J Rock Mech Min Sci 2011;48:1344–51. https://doi.org/10.1016/j.ijrmms.2011.09.014.

[11] Sato K, Isobe T, Mori N, Goto T. 9. Microseismic activity associated with hydraulic mining. Int J Rock Mech Min Sci Geomech Abstr 1986;23:85–94. https://doi.org/10.1016/0148-9062(86)91669-4.

[12] Saito A, Tsugawa T, Otsuka Y, Nishioka M, Iyemori T, Matsumura M, et al. Acoustic resonance and plasma depletion detected by GPS total electron content observation after the 2011 off the Pacific coast of Tohoku Earthquake. Earth, Planets Sp 2011;63:64. doi:10.5047/eps.2011.06.034.

[13] Han Y, Hu D, Matzar L. Numerical computation of elastic properties for porous rocks based on CT-scanned images using direct mapping method. J Pet Sci Eng 2014;122:346–53. doi:10.1016/j.petrol.2014.07.029.

[14] Hardy HR. Application of acoustic emission techniques to rock mechanics research. In: Liptai RG, Harris DO, Tatro CA, editors. Acoust. Emiss., West Conshohocken. PA: ASTM International; 1972. p. 41–83. doi:10.1520/STP35381S.

[15] Kusunose K, Lei X, Nishizawa O, Satoh T. Effect of grain size on fractal structure of acoustic emission hypocenter distribution in granitic rock. Phys Earth Planet Inter 1991;67:194–9. https://doi.org/10.1016/0031-9201(91)90070-X.

[16] Baud P, Klein E, Wong T. Compaction localization in porous sandstones: spatial evolution of damage and acoustic emission activity. J Struct Geol 2004;26:603–24. https://doi.org/10.1016/j.jsg.2003.09.002.

[17] Zhang SW, Shou KJ, Xian XF, Zhou JP, Liu GJ. Fractal characteristics and acoustic emission of anisotropic shale in Brazilian tests. Tunn Undergr Sp Technol 2018;71:298–308. https://doi.org/10.1016/j.tust.2017.08.031.

[18] Stoeckhert F, Molenda M, Brenne S, Alber M. Fracture propagation in sandstone and slate – laboratory experiments, acoustic emissions and fracture mechanics. J Rock Mech Geotech Eng 2015;7:237–49. https://doi.org/10.1016/j.jrmge.2015.03.011.

[19] Wang J, Xie L, Xie H, Ren L, He B, Li C, et al. Effect of layer orientation on acoustic emission characteristics of anisotropic shale in Brazilian tests. J Nat Gas Sci Eng 2016;36:1120–9. https://doi.org/10.1016/j.jngse.2016.03.046.

[20] Stamopoulos AG, Tserpes KI, Pantelakis SG. Multiscale finite element prediction of shear and flexural properties of porous CFRP laminates utilizing X-ray CT data. Theor Appl Fract Mech 2017. https://doi.org/10.1016/j.tafmec.2017.04.020.

[21] Zhao Y, Zhu G, Zhang C, Liu S, Elsworth D, Zhang T. Pore-Scale reconstruction and simulation of non-Darcy flow in synthetic porous rocks. J Geophys Res Solid Earth 2018;123:2770–86. doi:10.1002/2017JB015296.

[22] Mathews JP, Campbell QP, Xu H, Halleck P. A review of the application of X-ray computed tomography to the study of coal. Fuel 2017;209:10–24. https://doi.org/10.1016/j.fuel.2017.07.079.

[23] Shi X, Pan J, Hou Q, Jin Y, Wang Z, Niu Q, et al. Micrometer-scale fractures in coal related to coal rank based on micro-CT scanning and fractal theory. Fuel 2018;212:162–72. https://doi.org/10.1016/j.fuel.2017.09.115.

[24] Karacan CO, Okandan E. Adsorption and gas transport in coal microstructure: investigation and evaluation by quantitative X-ray CT imaging. Fuel 2001;80:509–20. https://doi.org/10.1016/S0016-2361(00)00112-5.

[25] Xing YK, Zhang GQ, Lin Q, Bu XQ, Da YP, Qi Y. Subcritical fracture process of sandstone with AE energy analysis. 51st US Rock Mech. Symp.. American Rock Mechanics Association; 2017.

[26] Kong X, Wang E, He X, Li D, Liu Q. Time-varying multifractal of acoustic emission about coal samples subjected to uniaxial compression. Chaos Solit Fract 2017;103:571–7. http://dx.doi.org/10.1016/j.chaos.2017.07.015.

[27] Xie H, Pariseau WG. Fractal character and mechanism of rock bursts. Int J Rock Mech Min Sci 1993;30:343–50. doi:10.1016/0148-9062(93)91718-X.

[28] ISRM. The complete ISRM suggested methods for rock characterization, testing and monitoring: 1974-2006. International Soc. for Rock Mechanics, Commission on Testing Methods; 2007.

[29] Song H, Jiang Y, Elsworth D, Zhao Y, Wang J, Liu B. Scale effects and strength anisotropy in coal. Int J Coal Geol 2018;195:37–46. doi:10.1016/J.COAL.2018.05.006.

[30] Song H, Zhao Y, Jiang Y, Zhang X. Influence of heterogeneity on the failure characteristics of coal under uniaxial compression condition. J China Coal Soc 2017;42:3125–32.

[31] Zhao Y, Zhao G-F, Jiang Y. Experimental and numerical modelling investigation on fracturing in coal under impact loads. Int J Fract 2013;183:63–80. doi:10.1007/s10704-013-9876-6.

[32] Cai YD, Liu DM, Pan ZJ, Yao YB, Li CC. Mineral occurrence and its impact on fracture generation in selected Qinshui basin coals: an experimental perspective. Int J Coal Geol 2015;150:35–50. doi:10.1016/j.coal.2015.08.006.

[33] Pomeroy CD, Hobbs DW, Mahmoud A. The effect of weakness-plane orientation on the fracture of Barnsley Hards by triaxial compression. Int J Rock Mech Min Sci Geomech Abstr 1971;8:227–38. https://doi.org/10.1016/0148-9062(71)90021-0.

[34] Nasseri MHB, Rao KS, Ramamurthy T. Anisotropic strength and deformational behavior of Himalayan schists. Int J Rock Mech Min Sci 2003;40:3–23. https://doi.org/10.1016/S1365-1609(02)00103-X.

[35] George JDS. Structural effects on the strength of New Zealand coal. Int J Rock Mech Min Sci 1997;34:299. e1-299.e11 https://doi.org/10.1016/S1365-1609(97)00184-6.

[36] Nasseri MHB, Mohanty B, Young RP. Fracture toughness measurements and acoustic emission activity in brittle rocks. Pure Appl Geophys 2006;163:917–45. doi:10.1007/s00024-006-0064-8.

[37] Vishal V, Ranjith PG, Singh TN. An experimental investigation on behaviour of coal under fluid saturation, using acoustic emission. J Nat Gas Sci Eng 2015;22. doi:10.1016/j.jngse.2014.12.020.

[38] Wu J, Zhang SH, Cao H, Kemeny J. The effect of pulse frequency on the acoustic emission characteristics in coal bed hydraulic fracturing. 50th US Rock Mech Symp; 2016.

[39] Pei J, Fei W, Liu J. Spatial evolution and fractal characteristics of natural fractures in marbles under uniaxial compression loading based on the source location technology of acoustic emission. Environ Earth Sci 2016;75:828. doi:10.1007/s12665-016-5649-7.

[40] Hoek E, Martin CD. Fracture initiation and propagation in intact rock - A review. J Rock Mech Geotech Eng 2014;6:287–300. doi:10.1016/j.jrmge.2014.06.001.

[41] Kirby GC, Mazur CJ. Fracture toughness testing of coal. 26th US Symp Rock Mech; 1985.

[42] Jaeger JC. Shear failure of Anistropic rocks. Geol Mag 1960;97:65–72. doi:10.1017/S0016756800061100.

[43] Carpinteri A, Corrado M, Lacidogna G. Heterogeneous materials in compression: correlations between absorbed, released and acoustic emission energies. Eng Fail Anal 2013;33:236–50. https://doi.org/10.1016/j.engfailanal.2013.05.016.

[44] Karakus M, Ingerson A, Thurlow W, Genockey M, Jones J. A new acoustic energy-based method to estimate pre-loads on cored rocks. In: Handb. res. trends digit. adv. eng. geol.. IGI Global; 2018. p. 281–325.

[45] Cho JW, Kim H, Jeon S, Min KB. Deformation and strength anisotropy of Asan gneiss, Boryeong shale, and Yeoncheon schist. Int J Rock Mech Min Sci 2012;50:158–69. doi:10.1016/j.ijrmms.2011.12.004.

[46] Carpinteri A, Lacidogna G, Niccolini G. Fractal analysis of damage detected in concrete structural elements under loading. Chaos Solit Fract 2009;42:2047–56. https://doi.org/10.1016/j.chaos.2009.03.165.

[47] Carpinteri A, Corrado M, Lacidogna G. Three different approaches for damage domain characterization in disordered materials: fractal energy density, b-value statistics, renormalization group theory. Mech Mater 2012;53:15–28. https://doi.org/10.1016/j.mechmat.2012.05.004.

[48] Iturrioz I, Lacidogna G, Carpinteri A. Acoustic emission detection in concrete specimens: experimental analysis and lattice model simulations. Int J Damage Mech 2014;23:327–58.

[49] Mandelbrot BB. Stochastic models for the earth's relief, the shape and the fractal dimension of the coastlines, and the number-area rule for islands. Proc Natl Acad Sci 1975;72(3825). LP–3828.

[50] Hirata T. A correlation between the b value and the fractal dimension of earthquakes. J Geophys Res 1989;94:7507–14. doi:10.1029/JB094iB06p07507.